



Dehydrogenation properties of ZnO and the impact of gold nanoparticles on the process



Patrycja Suchorska-Woźniak^a, Olga Rac^{a,*}, Roman Klimkiewicz^b, Marta Fiedot^a, Helena Teterycz^a

^a Faculty of Microsystem Electronics and Photonics, Wrocław University of Technology, Janiszewskiego 11/17, 50-372 Wrocław, Poland

^b Włodzimierz Trzebiatowski Institute of Low Temperature and Structure Research of the Polish Academy of Sciences, Okólna 2, 50-422 Wrocław, Poland

ARTICLE INFO

Article history:

Received 24 July 2015

Received in revised form

22 December 2015

Accepted 15 January 2016

Available online 19 January 2016

Keywords:

Catalysis

Dehydrogenation

Gold nanoparticles

Zinc oxide

ABSTRACT

The article presents the results of catalytic and surface properties of pure zinc oxide synthesized by hydrothermal method and surface-doped with gold nanoparticles. As a test reaction, the catalytic transformation of *n*-butyl alcohol towards the dehydrogenation or bimolecular condensation of symmetric ketone or an ester was studied. The tested materials catalyse both consecutive reactions, wherein the transformation towards the ketone is dependent on the presence of surface oxygen vacancies, whose concentration depends on the temperature. In turn, the transformation to the ester occurs in the presence of gold nanoparticles deposited on the surface of zinc oxide. The difference in work function of electrons from these materials create a change in the electron concentration in the surface area and will shift the balance of the coupling reaction of hydrogen with lattice oxygen, which prefers the formation of aldehyde and ester. The results were compared with the catalytic properties of other previously studied oxide systems in this group of changes. This analysis enabled the development of the mechanism of transformation and explanation of the impact of gold on the kinetics of the process.

© 2016 Elsevier B.V. All rights reserved.

1. Introduction

Zinc oxide is widely used in various areas of science and technology because of its physico-chemical and biological properties. It is an important material in electronics and electrical engineering [1–4]. Because of its stability, zinc oxide was used in the first chemical resistive gas sensors as a gas-sensitive material [5]. It is still used in sensors of various gases (H_2 , SF_6 , C_4H_{10} , C_2H_5OH) [6–8]. The temperature of gas sensors comprising zinc oxide as a sensor material is relatively high (400–500 °C), but if the sensors are made of nanometric particles, then the operating temperature decreases by approx. 200 °C [6]. The selectivity of the ZnO-based sensors is small but it can be improved by doping ZnO with various compounds. Among the dopes that significantly improve the sensors parameters, there are gold nanoparticles [9–11].

The catalytic properties of gold were noted by Bond et al. as early as in the 1970's [12,13]. They demonstrated that gold, although has inferior catalytic properties in comparison with metals such as platinum or palladium, it can catalyse hydrogenation, dehydro-

genation and hydrogen exchange reactions. The breakthrough was achieved by Haruta et al. who showed that gold particles scattered on transition metal oxides as carriers demonstrate significantly higher catalytic activity in the oxidation reaction of hydrogen and carbon monoxide [14,15], and by Nkosi et al. in the hydrochlorination reactions [16]. In recent years, the role of gold in catalysis has gained great importance [17–20].

Oxide sensor materials and phenomena occurring during gas detection are typical of heterogeneous catalysis. For this reason, the parameters of chemical resistance sensors, similarly to heterogeneous catalysts, are determined by the type, surface condition and microstructure of the material. Preparation and methods for characterization of materials in both cases are almost the same. Only the final stages of preparing these materials (as sensor or as catalytic materials) are different [21]. For these reasons, the authors started working on determining the catalytic properties of pure zinc oxide and zinc oxide surface-doped with gold in the transformation reaction of *n*-butyl alcohol. This material was prepared for chemical sensors for detection of low concentrations of volatile sulfur compounds.

The article presents not only the results of the catalytic properties of pure ZnO and ZnO doped with gold, but it also proposes the mechanism of the reactions taking place on the surface of

* Corresponding author.

E-mail address: olga.rac@pwr.edu.pl (O. Rac).

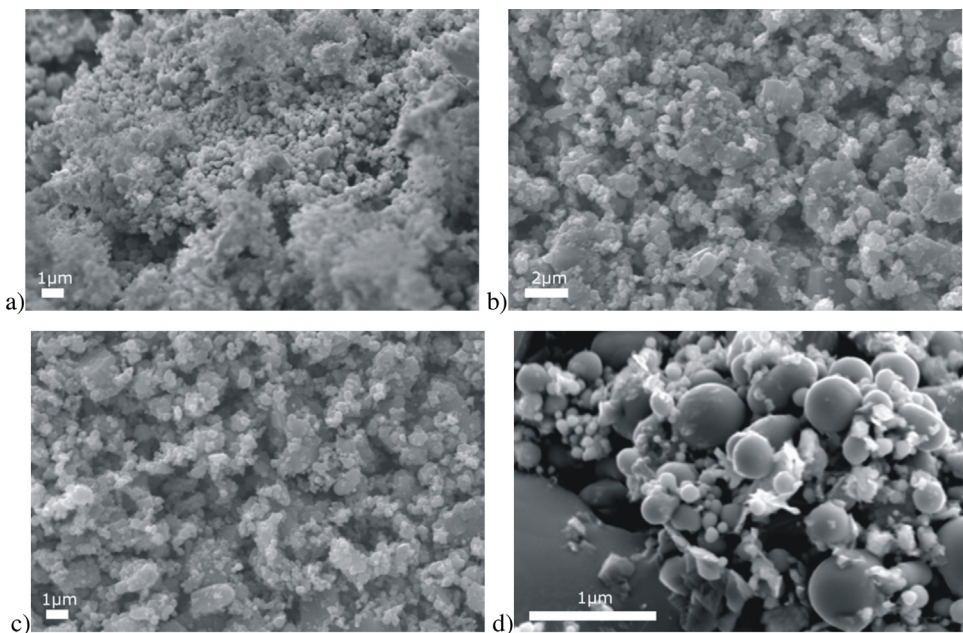


Fig. 1. Microstructure of (a) ZnO undoped after drying; ZnO containing 1% by weight Au: (b) before the reaction; (c) after the reaction at 460 °C; (d) SnO₂ after the reaction.

that catalyst. Dehydrogenation properties of zinc oxide have long been known [22,23], but publications relate to secondary alcohols [24–27] carboxylic acids [28] or dehydrogenation of primary structures [29] without consecutive reactions, i.e. bimolecular condensation towards the symmetric ketone [30] or ester [31,32]. Dehydration features [33] are also observed.

2. Experimental

The particles of zinc oxide were obtained by hydrothermal method. For this purpose, two aqueous solutions were prepared: 1 M zinc nitrate Zn(NO₃)₂ and 1 M solution of hexamethylenetetramine (HMT). These solutions were mixed in the 1:1 proportion and diluted with water to the final concentration of 100 mM. The reaction mixture containing both reactants was filtered and was heated at 90 °C for 6 h. Simultaneously, a series of Reactions (1)–(7) [34,35] occurred in the volume of the solution, resulting in microstructures of zinc oxide were formed.



The resulting ZnO suspension was filtered, and repeatedly rinsed with deionized water having a conductivity of 0.5 μS/cm.

The gold nanoparticles were synthesized by chemical reduction of gold ions in the aqueous solution in the presence of surfactant and polymer as stabilizers. For this purpose, solutions of: 0.08 M gold chloride (HAuCl₄), 0.06 M ascorbic acid, low molecular weight polyethyleneimine (PEI) having an average molecular weight of 10 kDa at a concentration of 43 g/dm³, and 0.08 M Triton® X-100 were prepared. The prepared solutions were mixed together in

such amounts that the final concentration of ions in the Au³⁺ solution was 1 mM, and the concentration of Triton® X-100 was 0.2% by weight. The molar ratio of PEI to chloroauric acid was 8:1 and the molar ratio of ascorbic acid to chloroauric acid was 1:1. Ascorbic acid was added to a solution containing the precursor of gold ions and stabilizers. The reduction of gold ions with ascorbic acid resulted in obtaining a colloidal solution of gold having a red colour.

Surface doping of zinc oxide with gold nanoparticles was performed by the process of reducing Au³⁺ gold ions in a suspension containing grains of zinc oxide (ZnO). For this purpose, a solution of surfactant, chloroauric acid and polyethyleneimine was added into the suspension of zinc oxide obtained by hydrothermal method and mixed. The content of gold ions in the solution relative to the weight of zinc oxide varied between 0% and 2% by weight. It was followed by reduction of gold ions with ascorbic acid, adding it slowly, portionwise. The resulting nanoparticles were deposited on the surface of the grains of zinc oxide. The resulting suspensions of zinc oxide powder doped with gold were centrifuged, rinsed several times with water in the decantation process and dried with a lyophilizer. Then, oxides were heated at 500 °C for 30 min in order to remove organic residues (PEI, Triton® X-100).

UV-vis spectroscopic measurements of the colloidal solutions of gold were performed using the Optizen Alpha Hybrid Mecasys spectrophotometer. Absorption spectra were recorded at room temperature in the wavelength range of 200–700 nm. Quartz cuvettes were used.

The size of the distribution of gold nanoparticles was determined by dynamic light scattering (DLS). Tests were performed using a Nicomp 380 ZLS (Particle Sizing Systems, USA) device with a laser having a 532 nm wavelength and a 50 mW power. The frequency of photon counting by autocorrelator was set at approximately 200 kHz, and a single measurement time was 3 min. In the measurements, a 40 × 10 × 10 mm polymethylmethacrylate (PMMA) cuvette was used.

The phase composition of the catalysts was determined on the basis of the diffraction patterns obtained using an X-ray Philips Materials Research Diffractometer (MRD) with monochromatic micro-focusing source of CuKα radiation. Typical powder materials were used, i.e. θ/2θ scan type.

The microstructure of zinc oxide particles was examined by the Zeiss EVO LS15 scanning electron microscope: acceleration voltage of 20 kV, sample current of 100 pA, equipped with an adapter for qualitative and quantitative analysis by the non-model method.

The substructure of gold nanoparticles was observed by the EM900 (Zeiss, Germany) transmission electron microscope (TEM). The magnification used was equal to 81000 \times . The samples were prepared by depositing drops of an aqueous dispersion of nanoparticles onto 300 copper mesh, coated with a layer of carbon and Formvar resin. The prepared samples were dried at ambient atmosphere for 45 min, and then subjected to a microscopic observation.

The surface chemistry of pure and Au-doped ZnO catalysts including their contaminations was characterized by XPS method using the SPECS XPS spectrometer working under ultrahigh vacuum conditions at 10 $^{-7}$ Pa maintained by the ion-sorption ultrahigh vacuum pump (IP-300 VARIAN model). It consists of vacuum chamber equipped, among other, with the sample XYZ manipulator (PREVAC SM-100 model), an X-ray source (Al-K α 1486.6 eV; XR-50 SPECS model) and a concentric hemispherical analyzer (PHOIBOS-100 SPECS model). The XPS survey spectra, XPS spectral windows, and XPS spectral lines of basic elements were recorded, and the registered binding-energy (BE) scale was calibrated using the Au4f_{7/2} peak at 84.0 eV. The analysis of XPS data was performed using the CASA XPS Software.

All the powders of ZnO pure and Au doped were pelleted at 80 MPa pressure, crushed and sifted until a homogeneous granulation of the catalysts was obtained (0.6–1.2 mm).

The catalytic activity of the new materials was studied in a fixed bed standard flow system at the atmospheric pressure and in temperature 400 °C and 460 °C with 1 h $^{-1}$ load. The vertical quartz reactor with 3 cm 3 catalyst bed was used. The studies on catalytic properties of zinc oxide compositions in the reactions of primary alcohols conversion were carried out with the use of *n*-butanol. No carrier gas was utilised. The substrate was fed in a continuous manner from the top of the reactor with the use of a micropump with the LHSV = 3.0 cm 3 /cm 3 h. The products of the reaction were analysed with the use of a HP MSD 59 mass spectroscope and HP 6890 gas chromatograph.

3. Results

The microstructure of zinc oxide before/after doping with gold and before/after the catalytic transformation of *n*-butanol was examined using the SEM. The comparative analysis of SEM images demonstrated that during the heating process, there is a change in the microstructure of zinc oxide. Pure and dried zinc oxide is composed of numerous grains having a spherical shape and a size within the range of from 0.1 μm to 2 μm (Fig. 1a). There are also visible larger structures having a hexagonal shape, and agglomerates of different sizes. After heating, the microstructure of pure and surface-doped zinc oxide slightly changed (Fig. 1b). The grains maintained an irregular shape, but also larger grains and agglomerates can be found. In contrast, the microstructure of these materials has not changed during the catalytic reaction of transforming *n*-butyl alcohol at 460 °C (Fig. 1c). Under the reaction conditions, the catalysts based on zinc oxide did not undergo a reduction, in contrast to the previously tested catalysts based on tin dioxide (Fig. 1d) [36].

XRD tests have shown that the crystallographic structure of tested catalysts is the same as the crystallographic structure of standard zinc oxide. The grains of zinc oxide crystallized in the wurtzite-type structure with hexagonal unit cell, space group of P63mc and lattice parameters $a=3.2501\text{ \AA}$ and $c=5.2071\text{ \AA}$. The pure ZnO was a partial amorphous but after the process the material becomes crystalline (Fig. 2a). The zinc oxide doped with nanopar-

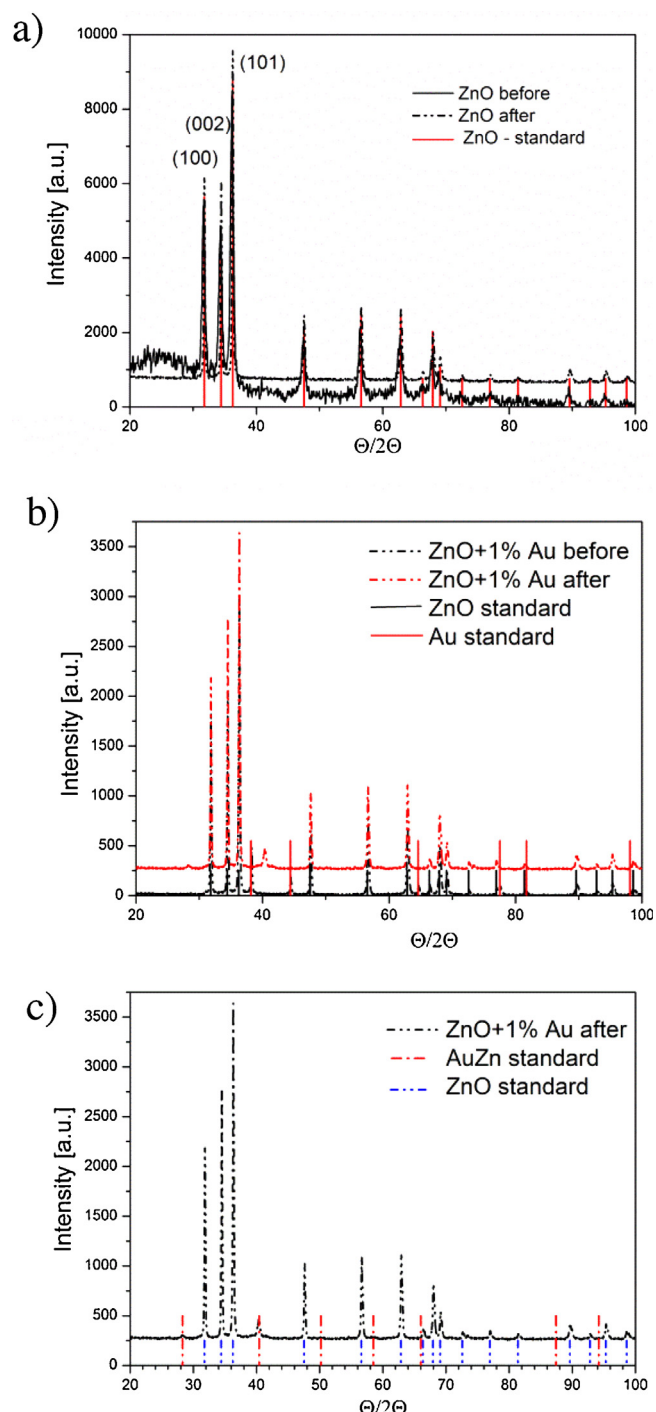


Fig. 2. X-ray diffraction pattern of catalysis materials: (a) zinc oxide before and after reaction; (b) zinc oxide doped 1% Au before and after reaction; (c) zinc oxide doped 1% Au after reaction and AuZn alloy.

ticles is more crystalline before reaction, because it is heated after the doping process (at 500 °C for 30 min) in order to remove organic residues (PEI, Triton® X-100). On diffraction patterns, no peaks characteristic for gold were observed, when its content is less than 1 wt.%. This is due to a very small average molecular size and large dispersion over the surface of the ZnO grains (Fig. 2b). The difference which exists between these two materials is the formation of alloy from interstitial zinc atoms with nanoparticles of gold (Fig. 2c).

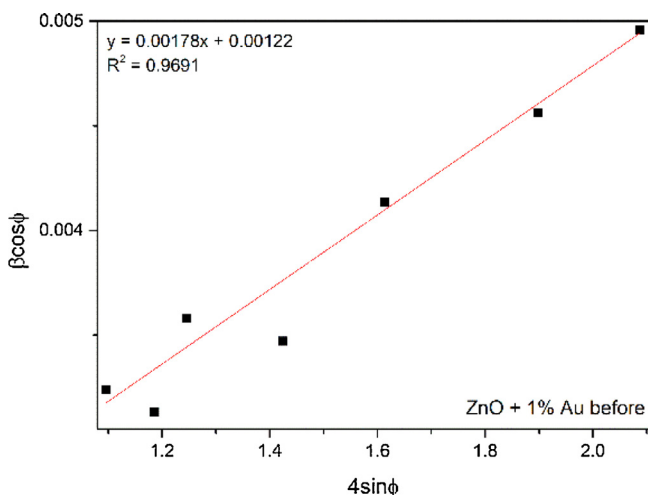


Fig. 3. The W–H analysis of ZnO + 1% Au before reaction.

By using of the Williamson–Hall (W–H) method (1) the average crystallite size and microstrains in ZnO were determined [37,38]:

$$\beta_{hkl} \cos(\phi) = \frac{k\lambda}{D_v} + 4\varepsilon \sin(\phi) \quad (1)$$

where:

β —half-width of the (FWHM) peak [rad],

ϕ —the angle of the highlight for the given band interference [rad],

k —the Scherrer constant (the 0.9 value),

λ —the length of the X-ray beam [nm],

D_v —the average crystallite size [nm],

ε —strain.

This equation represents Uniform Deformation Model (UDM) which takes into account uniform strain in all crystallographic directions, thus assuming the isotropic nature of analysed crystal. To calculate crystallite size and strain curve $\beta \cos \phi = f(4 \sin \phi)$ was plotted for preferred diffraction peaks (1 0 0), (0 0 2), (1 0 1), (1 0 2), (1 1 0), (1 0 3). The W–H analysis of zinc oxide doped with gold before reaction was demonstrated (Fig. 3).

Results clearly showed that crystallite size of the ZnO before the reaction was found to be 35 nm and that after reaction was 159 nm. This is due to the fact that analysed catalytic reaction takes place at an elevated temperature at which occurs recrystallization of ZnO. Moreover, after the reaction internal strains in the material are slightly reduced. This is because the reorganization of the structure at higher temperatures. Different situation is observed

Table 1
Strains and size of ZnO crystallites.

Sample	ε	D_v [nm]
ZnO before	0.00453	34.74
ZnO after	0.00426	158.88
ZnO + 1% Au before	0.00178	112.49
ZnO + 1% Au after	0.00275	571.35

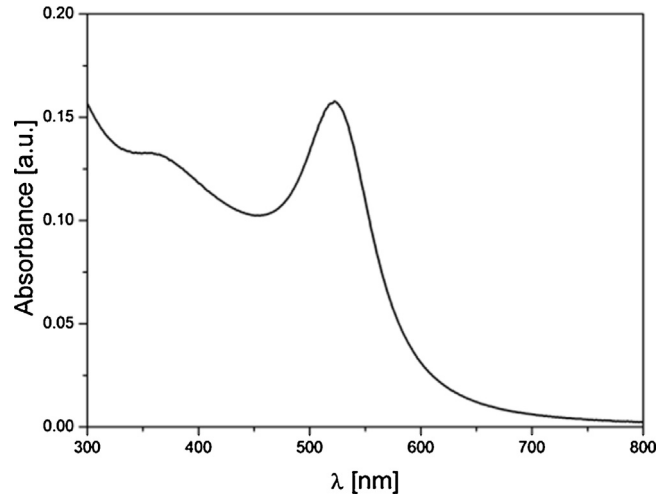


Fig. 4. UV–vis spectrum of gold nanoparticles.

in samples doped with gold nanoparticles. Such doped material has much larger size than the pure ZnO. It should be noted that the increase of the dimension of crystallites is caused by additional annealing of samples after the doping process. Similarly to the samples without dopant a several fold increase in size of crystallites is observed. The increase of strains after the reaction with *n*-butyl alcohol could be associated with the formation of Zn–Au alloy (Table 1).

In the UV–vis range, on the light absorption spectra of colloidal solutions of gold, there was observed a characteristic narrow peak at a radiation wavelength of 530 nm, which according to the Mie theory corresponds to nanoparticles having a diameter of not more than 10 nm (Fig. 4). These values are consistent with the values typical for the spherical forms of gold nanoparticles [39].

In order to confirm the results of the tests of the UV–vis radiation absorption, the average size of gold nanoparticles was determined by the dynamic light scattering (DLS) method. Studies have shown

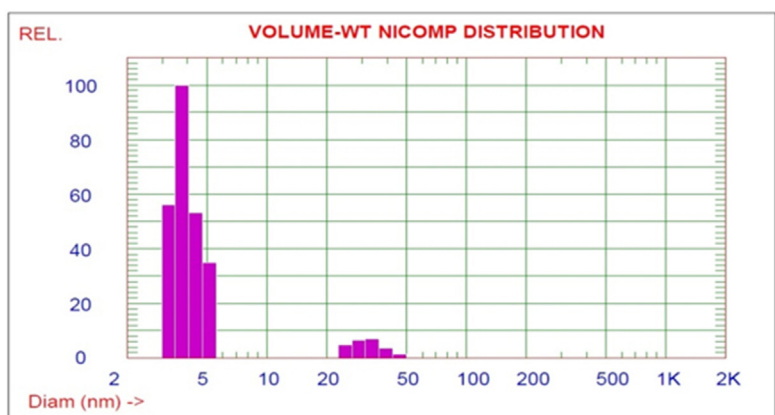


Fig. 5. Distribution of the size of gold nanoparticles performed by the DLS method.

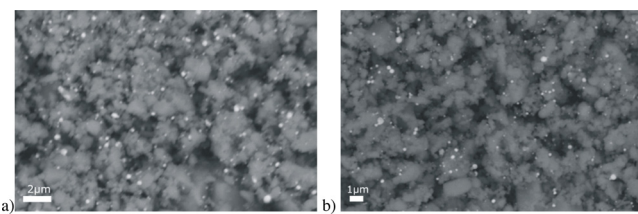


Fig. 6. The picture in atomic number contrast of ZnO powder with 2% wag. Au: (a) before reaction; (b) after reaction.

that the average particle size of the gold is approximately 4.0 nm for the vast majority of particles (93.5%) (Fig. 5).

On the basis of the results of the SEM and EDX tests, it was found that the surface of the ZnO grains there are gold particles having very different sizes, when their content is high (Figs. 6a and 7a). No presence of these particles was determined during the observation of powder containing only 0.25% by weight Au, which is caused by a large development of zinc oxide surface and highly uniform dispersion of gold nanoparticles (Fig. 7b). The distribution and size of the gold particles have not changed during the catalytic transformation of alcohol (Fig. 6b).

The XPS analysis was performed to determination of the surface chemistry. On the overall spectra strong contribution of basic elements of ZnO catalysts was observed from the core level Zn2p, O1s, C1s, Zn3s, Zn3p and Zn3d lines for Zn, reference line Au4f_{7/2} at 85.0 eV for gold and from C1s lines at BE ~286.0 eV for carbon (Fig. 8a). Weak trace of contribution of Au at the surface of Au-doped ZnO (Fig. 8b) is caused by the formation of alloy from interstitial zinc atoms with gold nanoparticles (Fig. 2c). Before reaction, for both catalysts pure and Au-doped ZnO, mainly on the surface O=C—OH bondings are observed. It is the residue after the synthesis of zinc oxide, which was used hexamethylenetetramine. After reaction on the both surfaces only C—OH bondings were detected. They are the remnants of the catalytic reaction products (Fig. 8c).

The catalytic properties of pure zinc oxide as well as zinc oxide surface-modified by gold nanoparticles were tested in the reactions of transformation of *n*-butyl alcohol. These reactions included dehydrogenation of aldehyde (butyraldehyde) and bimolecular condensation to ester (butyl butyrate), and ketone (heptan-4-one). These tests were carried out in a flow reactor at 1 h⁻¹ load at two temperatures of 400 °C and 460 °C. These results were compared with the results of other metal oxides used as catalysts in the same reaction.

The conversion rate of the transformation reaction of *n*-butyl alcohol conducted in the presence of catalysts based on zinc oxide depended on the temperature and the content of the dope (Fig. 9).

At 400 °C, the conversion rate in the presence of pure zinc oxide was only approximately 27%, and along with the increasing gold dopant, it increased to 60%. So, the presence of gold doubles the conversion. Since increasing the temperature by 60 °C resulted in a threefold increase in the conversion in the case of pure zinc oxide, the gold dopant catalytic effect manifested itself more evidently in respect of selectivity.

Also, large differences exist in the efficiency and selectivity (Figs. 10 and 11). At 400 °C, in the presence of pure zinc oxide, butyraldehyde is almost exclusively formed. When the ZnO catalyst is doped with gold, the total dehydrogenation efficiency is much higher, because the products contain little more aldehyde and a large amount of ester—the subsequent product of dehydrogenation (Tishchenko reaction) [31,32]. Ester efficiency values vary to a small degree along with the increasing dopant concentration above 0.5% by weight. When the gold content is 2%, ketone appears in the reaction products, which is also a subsequent product of dehydrogenation and bimolecular condensation (Fig. 10a). In contrast, at a temperature of 460 °C, the ketone is formed at all the tested catalysts, even in the undoped zinc oxide. In the doped catalysts, its efficiency is comparable to the efficiency of the ester (Fig. 10b). In this case, the total efficiency of the dehydrogenation products (aldehyde, ketone, ester) exceeds 90%.

The selectivity of the reaction in the presence of pure ZnO is very high compared to butyraldehyde. When ZnO is doped with Au, butyl butyrate is the product resulting from the additional expense of aldehyde at both temperatures. This reduces the selectivity to aldehyde by approximately 10% and 25%, respectively, at lower and higher temperatures. At 400 °C the selectivity of the butyl butyrate reaches the highest value when the dopant concentration is 0.5% by weight. (Fig. 11a). The ketone at the lower temperature is formed on the most active catalyst with a gold content of more than 1% by weight. At higher temperatures, the selectivity to the ketone is higher after the doping with gold, but it depends on the amount of the gold dopant when its content is more than 0.25% by weight. (Fig. 11b).

It is worth mentioning that high activity of ZnO surface-modified gold nanoparticles was observed in oxidation reactions both without and in the presence of UV radiation [40,41].

All the catalytic experiments were performed in the function of an increasing temperature. To check reproducibility, after an interruption of the experiments, cooling down the catalytic bed, the restarted system—after return to the starting parameters and then to the chosen temperature—enabled to obtain a satisfactory repetitiveness of results. For ZnO containing 1% by weight Au, at 460 °C, yields of butyraldehyde, butyl butyrate and heptan-4-one were 42%, 24%, 24% in the first run and 43%,

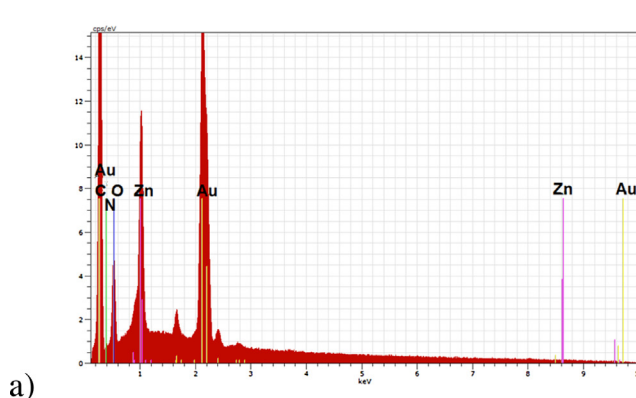


Fig. 7. The result of the EDX analysis: (a) the dependence of the intensity of the signal measurement on the energy of the electrons incident on the surface of zinc oxide doped with 0.5% weight gold nanoparticles; (b) the distribution of gold atoms over the surface of zinc oxide doped with gold nanoparticles.

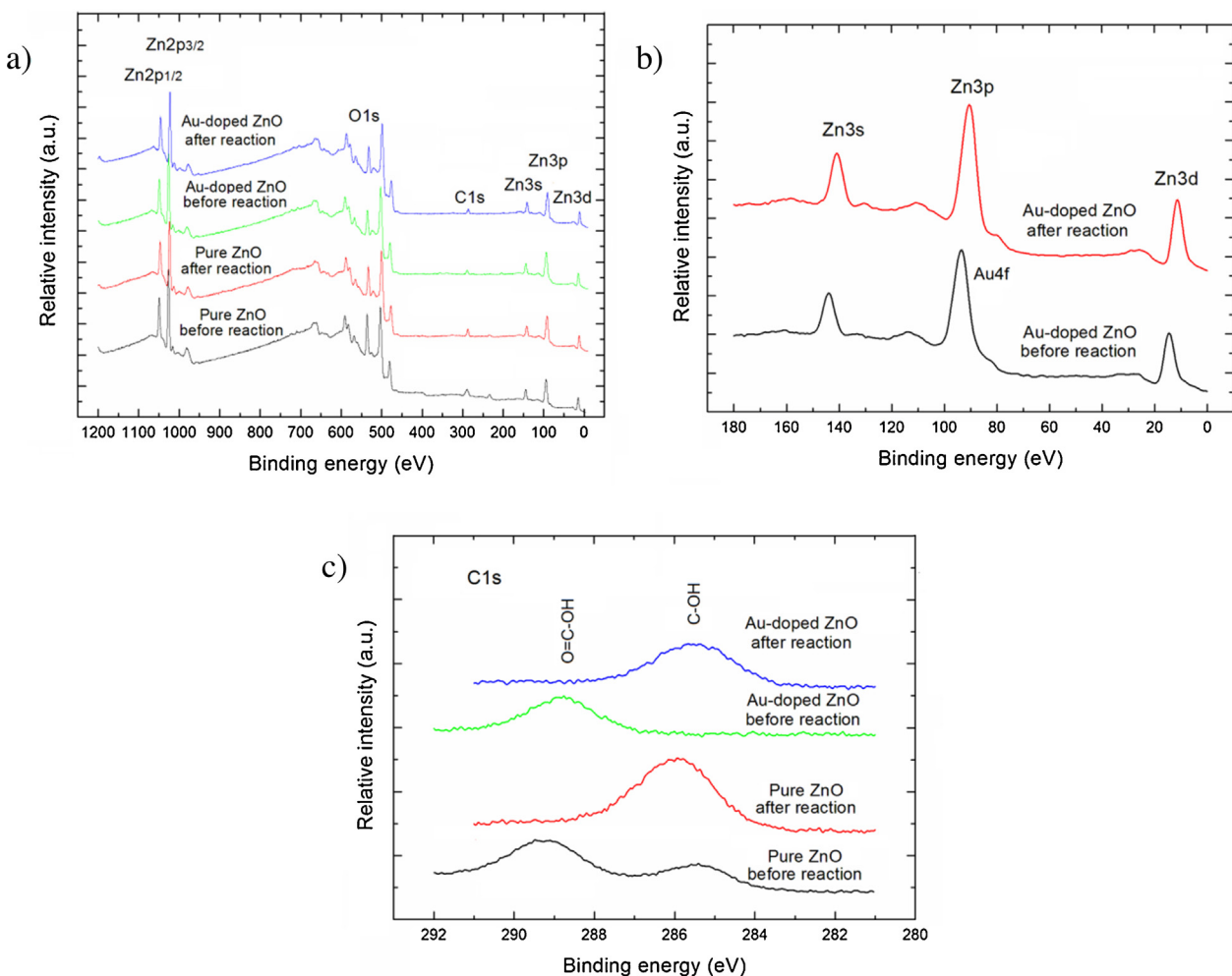


Fig. 8. The result of the XPS analysis: (a) overall spectra; (b) range spectra of core level for Au and Zn; (c) range spectra of core level for carbon C1s.

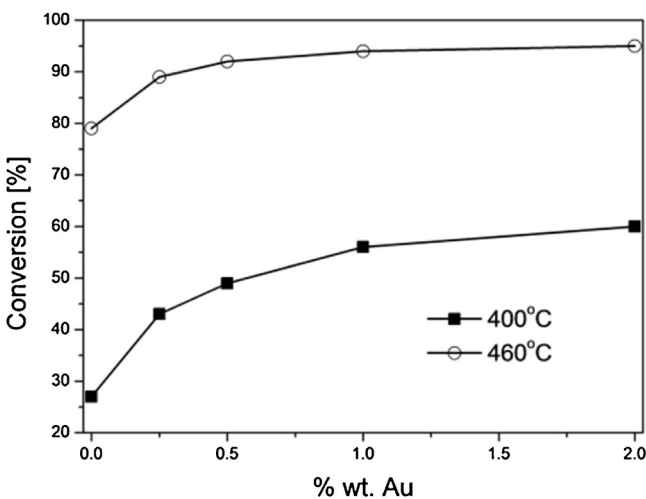


Fig. 9. The conversion rate of the transformation reaction of the *n*-butyl alcohol in the presence of the catalysts based on ZnO with different gold content. The reaction was carried out in a fixed bed standard flow system at the atmospheric pressure and in temperature 400 °C and 460 °C with 1 h⁻¹ load.

23%, 24% in the second run, respectively, at practically the same conversions.

Since no carbonaceous deposits were accumulated on the catalyst surface (Figs. 1c and 6b), it can be assumed that the car-

bon balance corresponds to the sum of unreacted butanol and the cumulative yield of distinguished dehydrogenation products. Therefore, at 400 °C and at 460 °C, the carbon balance ranges between 94–98% and 92–96%, respectively.

4. Discussion

The presented reaction of transformation of *n*-butyl alcohol occurs on the border of solid-gas phases. Its progress, and consequently the efficiency and selectivity depend not only on the structural characteristics, but also on the electrical properties of that material [42].

In the present study, pure zinc oxide and zinc oxide surface-doped with gold nanoparticles was used as a catalyst. Pure ZnO demonstrated high efficiency and selectivity in relation to the aldehyde at both temperatures (Figs. 10 and 11). In contrast, the material surface-doped with gold also catalysed the subsequent reaction to an ester with high selectivity and efficiency. At higher temperatures, i.e. 460 °C, the significant proportion of the ketone also made up a higher total selectivity and efficiency of dehydrogenation products, similar to the pure zinc oxide and the doped zinc oxide (Fig. 11).

The efficiency and selectivity of the reaction conducted in relation to the pure zinc oxide differed from the efficiency and selectivity of that process previously conducted on the catalysts created on the basis of tin dioxide [43], and stabilized zirconium dioxide (Fig. 12) [44]. The main difference in the results of the catal-

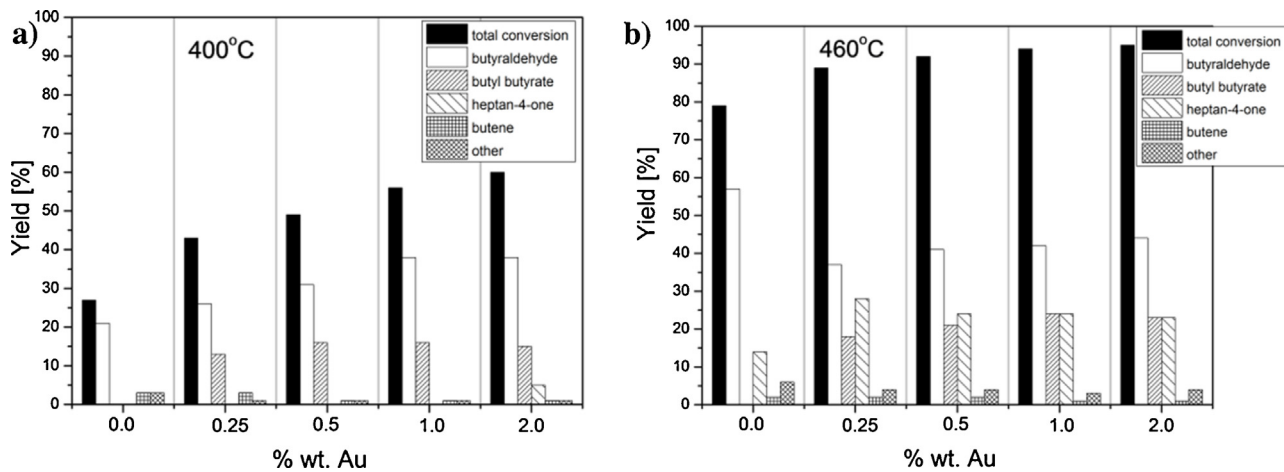


Fig. 10. The dependence of efficiency of the formation of aldehyde, ester, ketone and other (not analysed) products as a function of the amount of the Au dopant.

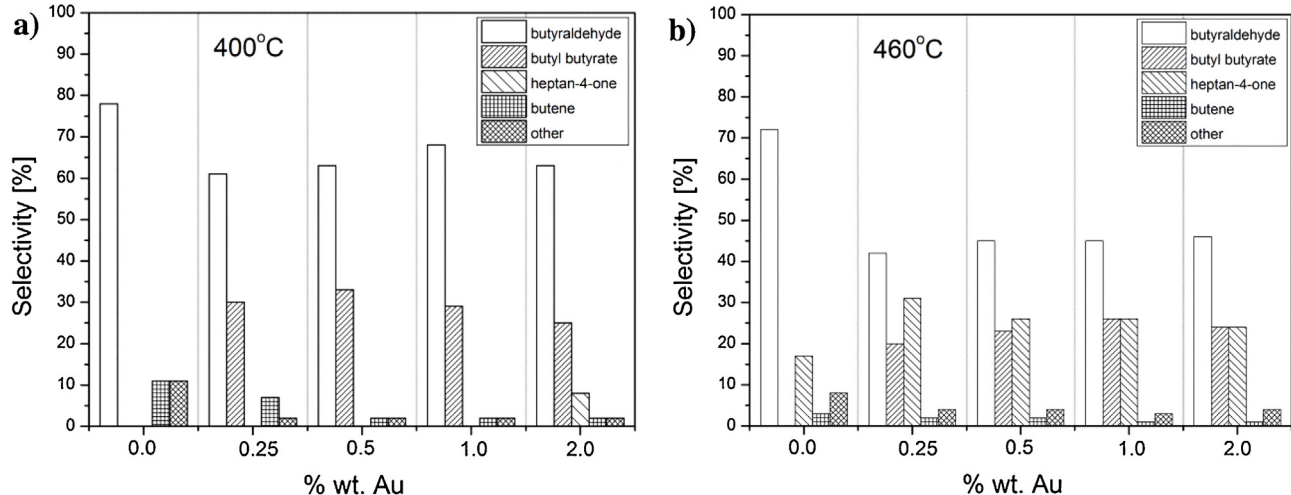


Fig. 11. The dependence of the selectivity of the formation of aldehyde, ester, ketone and other (not analysed) products as a function of the amount of the dopant.

ysis on the pure zinc oxide relative to the comparative materials is much higher selectivity to the aldehyde.

These previously tested oxides are the materials having the characteristics of the *n*-type semiconductors (SnO_2 , $\text{SnO}_2 + \text{CeO}_2$) or solid electrolytes (CeO_2 , ZrO_2 stabilized by MgO). At a temperature of 400°C , all these materials are characterized by both a higher efficiency and selectivity to the ketone than ZnO -based catalysts. The catalysts based on tin dioxide or stabilized by zirconium dioxide possess strong Lewis acid sites [44]. The presence of these centers is due to the existence of these materials in a number of surface oxygen vacancies [44]. Their concentration changes as a function of the partial gas pressure of oxygen in the ambient atmosphere and temperature. In the case of stabilized zirconium dioxide, their concentration depends only on the concentration of the stabilizing dopant. Oxygen vacancies are also present in zinc oxide. However, a unique feature of ZnO as the semiconductor photocatalyst is its open structure and the presence of the series of other structural defects in addition to oxygen vacancies [45,46].

Zinc oxide crystallizes in the wurtzite-type hexagonal structure, wherein the zinc atoms occupy half of the tetrahedral interstice created by oxygen atoms, and all octahedral interstice are empty. It is due to the numerous intrinsic defects occurring in the zinc oxide and the crystallization of this material in the form of a number of different microstructures, it is currently intensively studied in terms of applications in optoelectronics, sensor technique and

photocatalysis [47–49]. The formation of point defects with the ZnO structure causes the change of the ZnO volume and surface parameters [45,46].

These native point defects occurring in ZnO , which significantly affect its properties recorded in the Kröger–Vink notation include:

- zinc interstice (V_{Zn}''),
- oxygen interstice (V_0^{**}),
- zinc atoms in interstitial sites (Zn_i^{2+}),
- oxygen atoms in interstitial sites (O_i^{2-}),
- zinc atoms in place of oxygen (Zn_0^{***}),
- oxygen atoms in place of zinc ($\text{O}_{\text{Zn}}^{***}$).

In ZnO , there are also combinations of defects, e.g. Schottky pair (anion and cation interstice) and Frenkel pairs (cation gap and interstitial cation). The energy needed for the creation of the defect depends on the difference between the charge of the given defect and the charge on the lattice in which the defect is located. In ZnO , interstices and interstitial atoms have a charge of ± 2 , and antisite defect ± 4 [50].

According to some scientists, the dominant defects in the zinc oxide are oxygen vacancies [V_0^{**}]. In contrast, other authors believe that zinc is the dominant defect in the interstitial position Zn_i [51,52]. These defects result from the Frenkel and Schottky Reaction

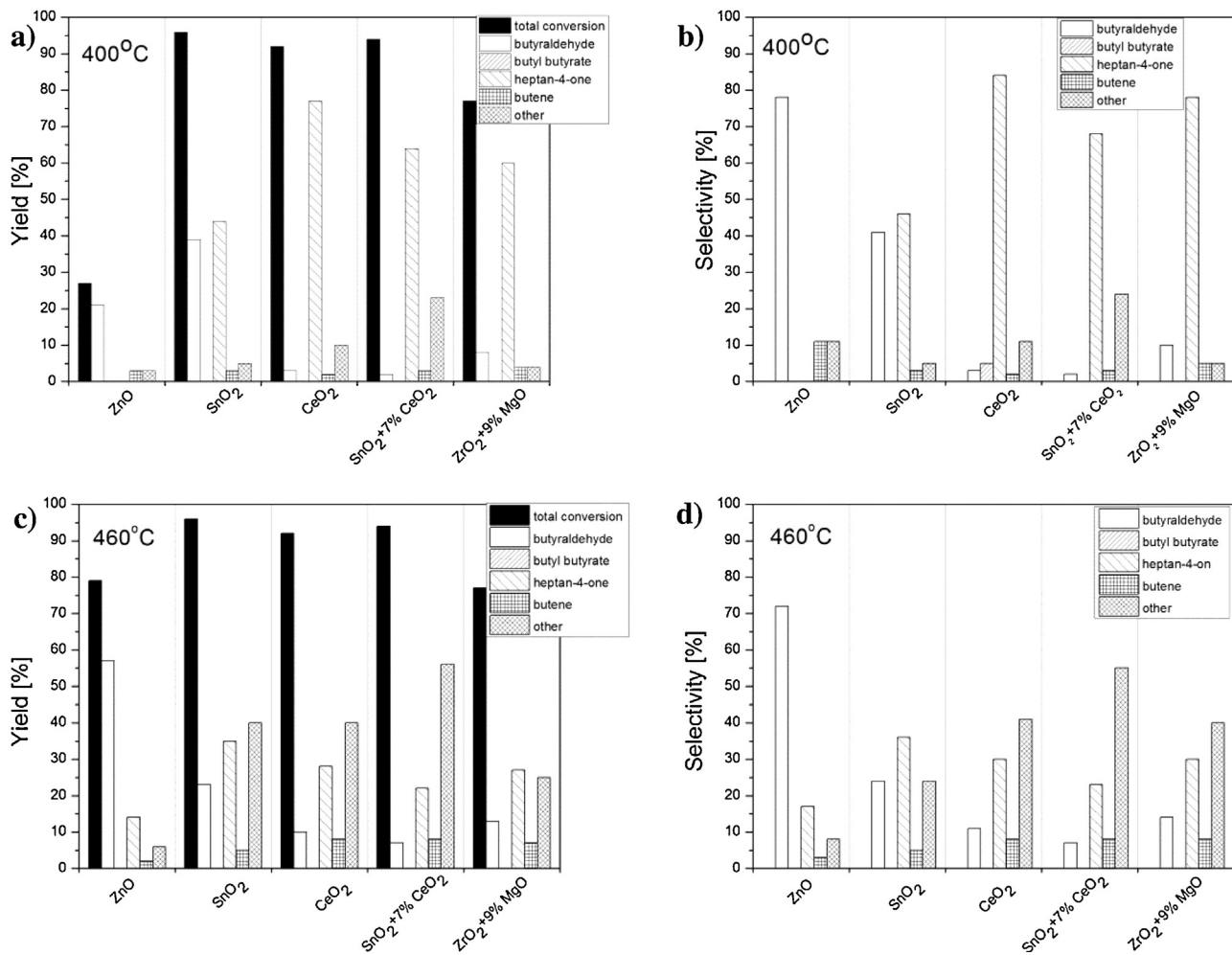


Fig. 12. The efficiency and selectivity of the condensation reaction of *n*-butanol in the presence of various oxides at: (a, b) 400 °C; (c, d) 460 °C.

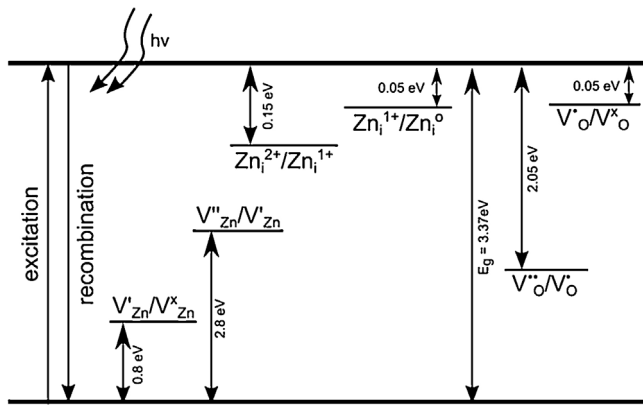
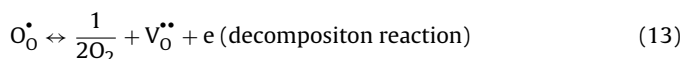
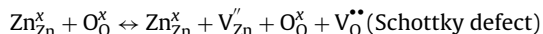
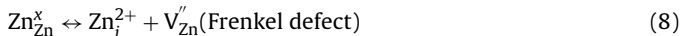
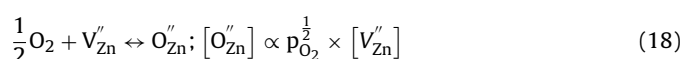
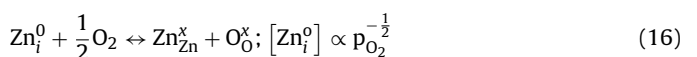
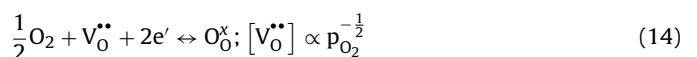


Fig. 13. Diagram of the energy levels resulting from the position arising from the presence of spotting defects in ZnO. To describe the diagram Kröger–Vink notations was used: i=interstitial site, Zn=zinc, O=oxygen, and V=vacancy. Superscript symbols indicate charges: a dot—negative charge, a prime—positive charge and a symbol x—zero charge.

(8)–(13) during the heat treatment of ZnO and cause the creation of the number of donor and acceptor levels in the band gap (Fig. 13).



The concentration of these major defects in ZnO depends on the oxygen gas pressure, and can be described by the following relationships (14)–(18) [53]:



where: $[\text{V}_\text{O}^{**}]$ and $[\text{V}_\text{Zn}'']$ is the concentration of non-ionized vacancies of oxygen and zinc, respectively. While $[\text{Zn}_i^0]$, $a[\text{O}_i^0]$ and $[\text{O}_\text{Zn}'']$ are concentrations of the interstitial zinc, the interstitial oxygen and another atom, i.e. oxygen in the zinc node. Eqs. (14)–(16) show

that the concentration of oxygen vacancies $[V_O^{\bullet\bullet}]$, zinc vacancies $[V_{Zn}^{\bullet}]$ and interstitial zinc $[Zn_i^0]$ increases as the oxygen pressure decreases p_{O_2} . In contrast, the other Eqs. (17) and (18) show that the concentration of the interstitial oxygen $[O_i^0]$ and oxygen in zinc ion nodes increases along with the increasing oxygen pressure p_{O_2} . Accordingly, heating in the anaerobic atmosphere, i.e. in the atmosphere, in which the reaction was conducted, causes an increase in the concentration of both the oxygen vacancies $[V_O^{\bullet\bullet}]$ and interstitial zinc $[Zn_i^0]$ and the atrophy of interstitial oxygen $[O_i^0]$ and oxygen in the zinc ion nodes.

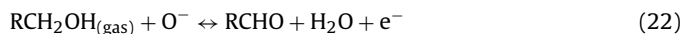
In the oxygen-containing atmosphere on the surface oxygen vacancies, oxygen undergoes physical and chemical adsorption (19).



As the temperature increases, the oxygen molecules ionize and dissociate (20)–(21).



In an atmosphere containing alcohol, the oxygen ions adsorbed on the surface vacancies may react in two ways, by undergoing dehydration (22) or dehydrogenation (23)–(24) [54,55].



In our studies, the reaction is carried out under anaerobic conditions at a temperature of 400 °C and 460 °C. The atmosphere contained only *n*-butyl alcohol. Under these conditions, the particles of alcohol may also be adsorbed on the surface vacancies of zinc oxide, which are the Lewis acid sites. These vacancies interact with the oxygen of the hydroxyl group. In contrast, the (electron-poor) carbon atom of the hydroxyl group becomes the center of the nucleophilic attack of nucleophilic agents which in these materials are surface (lattice) oxygen ions. This is consistent with the results obtained by Bielański and Haber [56].

In the first stage of the reaction, the adsorption of alcohol molecules takes place on the surface vacancies of the catalyst (Lewis acid sites), and the gradual dehydrogenation process (25)–(26) takes place. Hydrogen adsorbs on the electrophilic center (lattice oxygen) according to the Reaction (27) [21,57]. The resulting aldehyde is desorbed (28) or it reacts in the consecutive reaction with the intermediate product to form an ester (29). Groups may undergo the Reaction (30) to form hydrogen or may undergo the Reaction (31) to form water and oxygen vacancies. If this reaction takes place, zinc oxide will be reduced, similar to the catalysts based on tin or cerium dioxide [36].

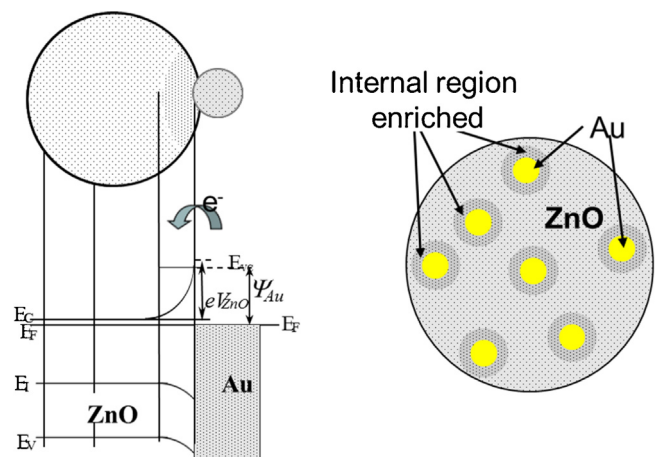


Fig. 14. The distribution pattern of gold nanoparticles on the surface of the zinc oxide grains.

At 400 °C, butene is one of the reaction products (in particular the reaction carried out in the presence of pure ZnO) (Fig. 10). This compound can be produced in the dehydration Reaction (32).



Taken into account that, under the reaction conditions, there is no modification in the microstructure and in the crystalline structure of zinc oxide, it should therefore be assumed that at this temperature there is no Reaction (31), because then it would result in the reduction of zinc oxide and an increase in the concentration of surface oxygen vacancies that significantly affect the kinetics of the tested process [44]. In addition, in the process of thermal decomposition, in the zinc oxide the excess zinc ions pass into the interstitial positions and migrate towards the surface. This migration of zinc ions also reduces the increase in the concentration of oxygen vacancies in the material. This is consistent with the literature data, which show that the thermal decomposition of zinc oxide takes place very slowly below 500 °C [58]. This cations migration is not observed in tin dioxide and cerium dioxide.

By analysing the catalytic properties of the gold particles deposited on the transition metal oxides, it is commonly believed that the dominant role is played by the oxygen molecules that dissociate on the surface of the gold [59,60]. At elevated temperatures, the atomic oxygen undergoes recombination to O_2 . The temperature of the recombination depends on the crystallographic orientation of the gold surface. It occurs on the surface of the polycrystalline Au at 650 K (377 °C) [55], on the gold surface having the Au (1 1 0) orientation it occurs at 590 K (317 °C) [61] and on the gold surface with the Au (1 0 0) orientation it occurs at 470 K (200 °C) [62]. In addition to this chemical aspect, the electronic aspect must also be taken into account [42].

Au nanoparticles randomly distributed on the surface of the ZnO particles cause the formation of the Schottky barriers between the metallic Au islands and the semiconductor ZnO. The work function of the electrons from zinc oxide—the *n*-type semiconductor ($\Phi_{ZnO} = 5.30$ eV) is different than in from noble metals ($\Phi_{Au} = 5.10$ eV, $\Phi_{Pt} = 5.65$ eV). Therefore, the Schottky barrier is formed at the interface of zinc oxide and gold. Since the Fermi levels of Au and ZnO must be balanced, the electrons pass from gold into ZnO [63]. Thus, the Au nanoparticles cause local changes in the Fermi level of zinc oxide [64]. As a result of this process, the Au islands become positively charged and the layer enriched with electrons (Fig. 14) is formed in the vicinity of the islands on the surface of the ZnO particles. For this reason, the conductance of the

ZnO grains modified with gold nanoparticles is greater than that of the pure ZnO.

The height of the Schottky barrier formed on the Au–ZnO border affects not only the process of the electric charge transportation, but also on the kinetics of the adsorption process in the area of the junction. In the metal-semiconductor boundary area, the crystalline structure of metal may also change, which also affects the adsorption process. In contrast, the height and width of the barrier may change due to the adsorption or desorption of gas molecules. In addition, gold is also known as the promoter of the catalytic dissociation of oxygen molecules, which is also known as a spillover phenomenon in the catalysis [65]. The resulting oxygen atoms migrate to the sensor surface and form oxygen ions that capture free electrons from the semiconductor. Since the reaction was carried out in an anaerobic atmosphere, the spillover phenomenon was not considered during the analysis of the occurring phenomena.

It is known that the ZnO activity towards the dehydrogenation or dehydration of alcohols is also dependent on the morphology [66]. In the present paper, zinc oxide was synthesized under the same conditions, and according to the microscopic observations, the structure of the catalysts was very similar. Moreover, the presence of gold nanoparticles on the surface of the grains is likely to partially reduce their sintering due to the high energy value of the phase boundary [67]. The microscopic observations confirmed the literature findings, since there was no change in the microstructure of ZnO during the reaction carried out at 460 °C (Fig. 1c). It was therefore assumed that the energy of the phase boundary between gold and zinc oxide has a significant impact on the properties of the tested catalysts.

By analyzing the impact of gold nanoparticles on the kinetics of the reaction, it was observed that at the temperature of 400 °C in the presence of pure ZnO, only the reaction of formation of the aldehyde (26) is preferred, whereas in the presence of the ZnO-based catalysts doped with gold, the reaction of formation of the aldehyde (26) and the consecutive reaction of formation of the ester (29) is preferred. Both of these reactions are dehydrogenation reactions. A thorough analysis of the proposed mechanism leads to the conclusion that the presence of Au nanoparticles shifts the equilibrium of the Reaction (27) to the left. Shifting the equilibrium is caused by the transition of electrons from gold to zinc oxide (Fig. 14). As a result, there is also a shift in the equilibrium Reaction (26) also to the left. As a consequence of these changes, the ester formation Reaction (29) may occur.

According to the Frost theory the junction metal/oxide disturbs the balance of ZnO defects [68]. Ghiotti et al. has been reported that cooper in Cu/ZnO catalyst for methanol synthesis is able to activate the CO molecule [69], but in case of Au/ZnO catalyst gold is not able to activate the support [70]. According to the above-presented theory the presence of gold nanoparticles do not disturb the balance of defects in ZnO but is a result of enriched layer formation (Fig. 14) at Au/ZnO boundary. Therefore the oxygen adsorbed in the region of enriched layer adjacent to the gold makes that nucleophilic attack of surface oxygen atoms is facilitated. Also, FTIR tests [70,71] shows that gold nanoparticles do not activate the oxidative dehydrogenation but modify the electrical properties of the zinc oxide.

At a temperature of 460 °C, in the ZnO-based catalysts, additional oxygen vacancies begin to form, which participate in the reaction of the ketone [28] formation. The reaction temperature (460 °C) is close to the temperature of thermal decomposition (above 500 °C) of zinc oxide [58]; furthermore, the reaction is carried out in an anaerobic atmosphere. In this atmosphere, according to the Reaction (14), the concentration of oxygen vacancies increases. In addition, in this reaction, electrons are produced that limit the impact of the electric potential of gold nanoparticles in the surface area (Fig. 8). Thus, the ketonization reaction that occurs

on ZnO is a consecutive reaction occurring at a higher temperature, because along with the increasing temperature, the concentration of the surface vacancies increases. However, an increase in their concentration is less than the one on the catalysts based on tin oxide, since in zinc oxide there is also the reaction of oxygen and interstitial zinc diffusion towards the surface of ZnO.

5. Conclusions

In the present study, the kinetics of the transformation of the n-butyl alcohol towards the dehydrogenation or bimolecular condensation in the presence of the catalysts based on zinc oxide and zinc oxide surface-doped with gold nanoparticles was investigated. Zinc oxide was synthesized by the hydrothermal method. The nanoparticles of gold were obtained by reduction of chloroauric acid (HAuCl_4) with ascorbic acid. As stabilizers in the reaction of gold reduction, we have used low-molecular polyethyleneimine (PEI) having an average molecular weight of 10 kDa and Triton® X-100. The reduction of the gold ions was carried out in a solution containing zinc oxide.

The obtained zinc oxide had the wurtzite-type crystalline structure and its structure did not change after doping with gold nanoparticles. The EDX studies demonstrated that the gold nanoparticles are uniformly dispersed on the surface of zinc oxide. There was no reduction of zinc oxide in the reaction conducted at the temperatures of 400 °C and 460 °C.

At a temperature of 400 °C in the presence of a pure zinc oxide, aldehyde is the main product of *n*-butyl alcohol transformation. By increasing the temperature to 460 °C, additionally the ketone was also the product. In the presence of zinc oxide doped with gold when the reaction is carried out at a 400 °C, then in addition to the aldehyde, ester also was created while in higher temperature aldehyde, ester and ketone were presented.

The catalytic properties of tested catalysts were compared with other previously studied oxides. In comparison with them, zinc oxide was characterized by a high selectivity of dehydrogenation to the aldehyde, but a low selectivity in relation to the ketone, where zinc oxide doped with gold had a high selectivity towards the ester.

Through the analysis of the literature and research results, the authors were able to develop a mechanism for this reaction and explain the impact of gold on the kinetics of the process. Due to the difference in their work function, the electrons from the gold particles pass to zinc oxide. This causes the shift to the left of the equilibrium of joining hydrogen and lattice oxygen. Consequently, in the presence of the ZnO-based catalysts doped with Au, the dehydrogenation and the formation of aldehyde and the consecutive reaction of ester formation is preferred.

The differences in the catalytic activity of zinc oxide and tin oxides have also been discovered by testing their sensory properties, in an atmosphere of 1-butanol and butanal [49]. When examining the composition of the gas atmosphere during sensors operation, the authors found that on the sensor surface of the zinc oxide layer, the intensive dehydrogenation of butanol into butanal occurs. In contrast, they had suggested that esters may be formed by further oxidation of butanal to butanoic acid and the subsequent esterification with butanol to form the butyl ester of butanoic acid. The authors of this article observed this behaviour when they applied zinc oxide doped with gold nanoparticles as a catalyst.

Acknowledgements

The project was funded by the National Science Centre based on Decision Number DEC-2012/07/N/ST7/02304 and from Funds for Science during 2014–2015 for Project No. 0067 W12.

References

- [1] S. Mansouri, R. Bourguiga, F. Yakuphanoglu, *Curr. Appl. Phys.* 12 (2012) 1619–1623.
- [2] K.D. Gunaratne, C. Berkdemir, C.L. Harmon, A.W. Castelman Jr., *J. Phys. Chem. A* 116 (2012) 12429–12437.
- [3] M. Purica, E. Budianu, E. Rusu, *Thin Solid Films* 383 (2001) 284–286.
- [4] T. Aoki, Y. Hatanaka, D.C. Look, *Appl. Phys. Lett.* 76 (2000) 3257–3258.
- [5] T. Seiyama, A. Kato, K. Fujishi, M. Nagatani, *Anal. Chem.* 34 (1962) 1502–1507.
- [6] S. Roy, S. Basu, *Bull. Mater. Sci.* 25 (2002) 513–515.
- [7] K.V. Gurav, P.R. Deshmukh, C.D. Lokhande, *Sens. Actuators B* 151 (2011) 365–369.
- [8] L. Wang, Y. Kang, X. Liu, S. Zhang, W. Huang, S. Wang, *Sens. Actuators B* 162 (2012) 237–243.
- [9] N.L. Hung, H. Kim, S.K. Hong, D. Kim, *Sens. Actuators B* 151 (2010) 127–132.
- [10] J. Guo, J. Zhang, M. Zhu, D. Ju, H. Xu, B. Cao, *Sens. Actuators B* 199 (2014) 339–345.
- [11] P. Rai, Y.S. Kim, H.M. Song, M.K. Song, Y.T. Yu, *Sens. Actuators B* 165 (2012) 133–142.
- [12] G.C. Bond, P.A. Sermon, G. Webb, D.A. Buchanan, P.B. Wells, *J. Chem. Soc. Chem. Commun.* (1973) 444–445.
- [13] P.A. Sermon, G.C. Bond, P.B. Wells, *J. Chem. Soc. Faraday Trans.* 75 (1979) 385–394.
- [14] M. Haruta, T. Kobayashi, H. Sano, N. Yamada, *Chem. Lett.* 16 (1987) 405–408.
- [15] M. Haruta, N. Yamada, T. Kobayashi, S. Iijima, *J. Catal.* 115 (1989) 301–309.
- [16] B. Nkosi, N.J. Coville, G.J. Hutchings, *Appl. Catal.* 43 (1988) 33–39.
- [17] G.C. Bond, D.T. Thompson, *Cat. Rev. Sci. Eng.* 41 (1999) 319–388.
- [18] G.J. Hutchings, *Catal. Today* 100 (2005) 55–61.
- [19] G.J. Hutchings, M. Haruta, *Appl. Catal. A* 291 (2005) 2–5.
- [20] O. Martin, C. Mondelli, D. Curulla-Ferré, C. Drouilly, R. Hauert, J. Pérez-Ramírez, *ACS Catal.* 5 (2015) 5607–5616.
- [21] D. Kohl, *J. Phys. D: Appl. Phys.* 34 (2001) 125–149.
- [22] W.A. Lazier, H. Adkins, *J. Am. Chem. Soc.* 47 (1925) 1719–1722.
- [23] S.M. Hosseini-Sarvari, *Curr. Org. Synth.* 10 (2013) 697–723.
- [24] S.M. Chaudhari, A.S. Waghulde, V. Samuel, M.L. Bari, V.R. Chumbhare, *Res. J. Chem. Sci.* 3 (2013) 38–44.
- [25] G. Djéga-Mariadassou, L. Davignon, A.R. Marques, *J. Chem. Soc. Faraday Trans.* 78 (1982) 2447–2454.
- [26] H.R. Mardania, M. Forouzania, M. Ziaria, A. Malekzadeh, P. Biparvac, *Chem. Commun.* 3 (2015) 199–207.
- [27] L. Saad, M. Riad, *J. Serb. Chem. Soc.* 73 (2008) 997–1009.
- [28] M. Gliński, G. Zalewski, E. Burno, A. Jerzak, *Appl. Catal. A* 470 (2014) 278–284.
- [29] V.K. Raizada, V.S. Tripathi, D. Lal, G.S. Singh, C.D. Dwivedi, A.K. Sen, *J. Chem. Technol. Biotechnol.* 56 (1993) 265–270.
- [30] M.J.L. Gines, E. Iglesia, *J. Catal.* 176 (1998) 155–172.
- [31] W.L. Chen, H.C. Liu, *Chin. Sci. Bull.* 60 (2015) 1–12.
- [32] B. Xu, J. Haubrich, C.G. Freysschlag, R.J. Madix, C.M. Friend, *Chem. Sci.* 1 (2010) 310–314.
- [33] I. Fatimah, Proceeding of International Conference On Research, Implementation And Education Of Mathematics And Sciences 2014, Yogyakarta State University, 18–20 May 2014, 79–86.
- [34] L. Vayssières, *Adv. Mater.* 15 (2003) 464–466.
- [35] Q.C. Li, V. Kumar, Y. Li, H.T. Zhang, T.J. Mark, R.P.H. Chang, *Chem. Mater.* 17 (2005) 1001–1006.
- [36] H. Teterycz, R. Klimkiewicz, B. Licznerski, Conference proceedings of 26th International Spring Seminar on Electronics Technology, ISSE 2003, Piscataway, NJ : IEEE (2003) 379–383.
- [37] G.K. Williamson, W.H. Hall, *Acta Metall.* 1 (1953) 22–31.
- [38] R. Yogamalar, R. Srinivasan, A. Vinu, K. Ariga, A. Chandra Bose, *Solid State Commun.* 149 (2009) 1919–1923.
- [39] P.K. Jain, K.S. Lee, I.H. El-Sayed, M.A. El-Sayed, *J. Phys. Chem. B* 110 (2006) 7238–7248.
- [40] S.A.C. Carabineiro, B.F. Machado, R.R. Bacsa, P. Serp, G. Drazic, J.L. Faria, J.L. Figueiredo, *J. Catal.* 273 (2010) 191–198.
- [41] C.G. Silva, M.J. Sampaio, S.A.C. Carabineiro, J.W.L. Oliveira, D.L. Baptista, R. Bacsa, B.F. Machado, P. Serp, J.L. Figueiredo, A.M.T. Silva, J.L. Faria, *J. Catal.* 316 (2014) 182–190.
- [42] T. Wolkenstein, *Adv. Catal.* 12 (1960) 189–264.
- [43] H. Teterycz, R. Klimkiewicz, M. Łaniecki, *Appl. Catal. A* 274 (2004) 49–60.
- [44] H. Teterycz, R. Klimkiewicz, M. Łaniecki, *Appl. Catal. A* 249 (2003) 313–326.
- [45] L. Schmidt-Mende, J.L. Mac Manus-Driscoll, *Mater. Today* 10 (2007) 40–48.
- [46] M.D. McCluskey, S.J. Jokela, *J. Appl. Phys.* 106 071101 (2009) 1–13.
- [47] Ü. Özgür, Y.I. Alivov, C. Liu, A. Teke, M.A. Reshchikov, S. Doğan, V. Avrutin, S.J. Cho, H. Morkoç, *J. Appl. Phys.* 98 (2005) 1–103.
- [48] A. Kołodziejczak-Radzimska, T. Jesionowski, *Materials* 7 (2014) 2833–2881.
- [49] B.P.J. de Lacy Costello, R.J. Ewen, P.R.H. Jones, N.M. Ratcliffe, R.K.M. Wat, *Sens. Actuators B* 61 (1999) 199–207.
- [50] J. Han, Y. Liu, N. Singhal, L. Wang, W. Gao, *Biochem. Eng. J.* 213 (2012) 150–162.
- [51] K.I. Hagemark, *J. Solid State Chem.* 16 (1976) 293–299.
- [52] M.H. Sukkar, H.L. Tuller, *Adv. Ceram.* 7 (1984) 71–90.
- [53] B. Lin, Z. Fu, Y. Jia, *Appl. Phys. Lett.* 79 (2001) 943–945.
- [54] M.A. Bartea, R.J. Madix, *J. Chem. Phys.* 74 (1981) 4144–4149.
- [55] N.D.S. Canning, D.A. Outka, R.J. Madix, *Surf. Sci.* 141 (1984) 240–254.
- [56] A. Bielanski, J. Haber, *Catal. Rev. Sci. Eng.* 19 (1979) 1–41.
- [57] G. Heiland, D. Kohl, *Chem. Sens. Technol.* 1 (1988) 15–38.
- [58] M. Kobayashi, M. Flytzani-Stephanopoulos, *Ind. Eng. Chem. Res.* 41 (2002) 3115–3123.
- [59] R. Meyer, C. Lemire, Sh. K. Shaikhutdinov, H.J. Freund, *Gold Bull.* 37 (2004) 72–124.
- [60] T.V.W. Janssens, B.S. Clausen, B. Hvolbæk, H. Falsig, C.H. Christensen, T. Bligaard, J.K. Nørskov, *Top. Catal.* 44 (2007) 15–26.
- [61] D.A. Outka, R.J. Madix, *Surf. Sci.* 179 (1987) 351–360.
- [62] J.M. Gottfried, N. Elghobashi, S.L.M. Schroeder, K. Christmann, *Surf. Sci.* 523 (2003) 89–102.
- [63] L. Sun, D. Zhao, Z. Song, C. Shan, Z. Zhang, B. Li, D. Shen, *J. Colloid Interface Sci.* 363 (2011) 175–181.
- [64] F. Flores, R. Miranda, *Adv. Mater.* 6 (1994) 540–548.
- [65] C. Li, L. Li, Z. Du, H. Yu, Y. Xiang, Y. Li, Y. Cai, T. Wang, *Nanotechnology* 19 (2008) 1–4.
- [66] W.H. Hirschwald, *Acc. Chem. Res.* 18 (1985) 228–234.
- [67] L.F. Gutiérrez, S. Hamoudi, K. Belkacem, *Catalysts* 1 (2011) 97–154.
- [68] J.C. Frost, *Nature* 334 (1988) 577–580.
- [69] G. Ghiorri, F. Bocuzzi, A. Chiòrino, *J. Chem. Soc. Chem. Commun.* (1985) 1012–1014.
- [70] M. Manzoli, A. Chiòrino, F. Bocuzzi, *Appl. Catal. B* 57 (2004) 201–209.
- [71] F. Bocuzzi, A. Chiòrino, S. Tsubota, M. Haruta, *Sens. Actuators B* 24–25 (1995) 540–543.